Freezing of the Lattice in the Kagome Lattice Heisenberg Antiferromagnet Zn-Barlowite $ZnCu_3(OD)_6FBr$

Jiaming Wang,[1] Weishi Yuan,[1] Philip M. Singer,[2] Rebecca W. Smaha,[3,4] Wei He,[3,5] Jiajia Wen,[3] Young S. Lee,[3,6] and Takashi Imai[1]

[1]*Department of Physics and Astronomy, McMaster University, Hamilton, Ontario L8S 4M1, Canada*
[2]*Department of Chemical and Biomolecular Engineering, Rice University, Houston, Texas 77005, USA*
[3]*Stanford Institute for Materials and Energy Sciences, SLAC National Accelerator Laboratory, Menlo Park, California 94025, USA*
[4]*Department of Chemistry, Stanford University, Stanford, California 94305, USA*
[5]*Department of Materials Science and Engineering, Stanford University, Stanford, California 94305, USA*
[6]*Department of Applied Physics, Stanford University, Stanford, California 94305, USA*

(Received 3 January 2022; accepted 28 February 2022; published 12 April 2022)

We use ^{79}Br nuclear quadrupole resonance (NQR) to demonstrate that ultraslow lattice dynamics set in below the temperature scale set by the Cu-Cu superexchange interaction J ($\simeq$160 K) in the kagome lattice Heisenberg antiferromagnet Zn-barlowite. The lattice completely freezes below 50 K, and ^{79}Br NQR line shapes become twice broader due to increased lattice distortions. Moreover, the frozen lattice exhibits an oscillatory component in the transverse spin echo decay, a typical signature of pairing of nuclear spins by indirect nuclear spin-spin interaction. This indicates that some Br sites form structural dimers via a pair of kagome Cu sites prior to the gradual emergence of spin singlets below ~30 K. Our findings underscore the significant roles played by subtle structural distortions in determining the nature of the disordered magnetic ground state of the kagome lattice.

DOI: 10.1103/PhysRevLett.128.157202

Identifying the spin liquid ground state realized in model spin Hamiltonians is the holy grail in the research field of frustrated magnetism [1,2]. Theoretically, multiple states often compete with each other for the ground state of a given spin Hamiltonian. This makes theoretical identification of the ground state a nontrivial problem. Likewise, on the experimental side, each spin liquid candidate material has its own complications, too, often arising from structural disorders. For example, the nonmagnetic interlayer Zn^{2+} sites of the kagome lattice Heisenberg antiferromagnet herbertsmithite $ZnCu_3(OH)_6Cl_2$ [3–17] and Zn-barlowite $ZnCu_3(OH)_6FBr$ [15,18–23] are occupied by Cu^{2+} defect spins with ~15% [5] and ~5% [20] probability, respectively. These defect spins have generally been believed to account for the enhanced magnetic response observed at low temperatures and mask the intrinsic behavior of the kagome planes.

In addition, recent theoretical works suggest that inhomogeneity in the magnitude of the Cu-Cu superexchange interaction J (= 160 K [19] ~190 K [4]) alone could significantly impact the nature of the ground state and induce spin singlets with inhomogeneous gaps, accompanied by orphaned localized spins elsewhere within the kagome planes [24–26]. Moreover, these orphaned spins may account for the enhanced magnetic response at low temperatures [24–26], even if there are no interlayer Cu^{2+} defect spins or spin vacancies [27] within the kagome planes. In fact, our recent ^{63}Cu nuclear quadrupole resonance (NQR) experiments established that spin singlets gradually emerge with inhomogeneous gaps below ~30 K in both herbertsmithite and Zn-barlowite [15].

Motivated by these developments, we explore the structural disorder and their dynamics in Zn-barlowite $ZnCu_3(OD)_6FBr$ based on NQR at ^{79}Br sites (nuclear spin 3/2). The ^{79}Br NQR frequency $^{79}\nu_Q$ and its distribution probe the local lattice environment and its disorder through the electric field gradient (EFG), while the nuclear spin-lattice $^{79}1/T_1$ and spin-spin $^{79}1/T_2$ relaxation rate shed light on the slow dynamics of the lattice at the timescale set by the inverse of the resonant frequency, $^{79}\nu_Q^{-1} \sim 0.04$ μs. We will demonstrate that ultraslow lattice dynamics set in below the temperature scale of $J \sim 160$ K, and the lattice freezes below ~50 K with enhanced structural disorder. Moreover, we will report our discovery of an oscillating component in the spin echo decay curves $M(2\tau) \sim \cos\{\omega_o(2\tau)\}$ [28–31] induced by indirect nuclear spin-spin interaction $\hbar a_{ij}\hat{\mathbf{I}}_i \cdot \hat{\mathbf{I}}_j$ [32–35], where τ is the separation time between 90° and 180° radio frequency pulses, $M(2\tau)$ is the spin echo amplitude at time 2τ, $\hat{\mathbf{I}}_i$ and $\hat{\mathbf{I}}_j$ are the nuclear spin operator at the ith and jth sites, and $a_{ij}(\sim\omega_o))$ is the indirect nuclear spin-spin coupling. In short, the spin echo amplitude oscillates, because nuclear spin $\hat{\mathbf{I}}_i$ precesses about the hyperfine magnetic field generated by

nuclear spin $\hat{\mathbf{I}}_j$, and vice versa. Such oscillations are a typical NMR signature of the pairing of atoms in molecules [28] and solids, including Cu-Cu spin singlet dimers in $SrCu_2(BO_3)_2$ [30] and $Cu_2Sc_2Mg_4O_{13}$ [31], but unexpected for the kagome lattice in Zn-barlowite. Our finding indicates that some ^{79}Br sites in the frozen lattice form structural dimers encompassing a pair of kagome Cu spin singlets. The existence of the oscillation with a well defined frequency contrasts with the Gaussian form of spin echo decay $M(2\tau)$ observed for the two-leg Heisenberg ladder in $SrCu_2O_3$ [36] and $Sr_{14}Cu_{24}O_{41}$ [37], in which spin singlets are entangled along the legs in the ladder. We will explain that the spin echo amplitude oscillation can be used as a probe of entanglement between spin singlets.

In Figs. 1, 2(a), and 2(b), we present the crystal structure of Zn-barlowite and representative ^{79}Br NQR line shapes. We refer readers to [15] and the Supplemental Material [38] for the entire ^{79,81}Br and ^{63,65}Cu NQR line shapes. We summarize the temperature dependence of the main peak frequency $^{79}\nu_Q^{\mathrm{Main}}$ in Fig. 3(a). Above 100 K, we found $^{79}\nu_Q^{\mathrm{Main}} \gtrsim 28.8$ MHz, accompanied by two additional small humps at $^{79}\nu_Q^A \simeq 28.2$ and $^{79}\nu_Q^B \simeq 29.4$ MHz [38]. NQR is a local probe, and this indicates that at least three slightly different structural environments exist for ^{79}Br sites. Previously, we identified three sets of ^{2}D [9] and ^{17}O [10] NMR signals for deuterated herbertsmithite as the main, the nearest neighbor (nn), and the twice more abundant next nearest neighbor (nnn) sites of the interlayer Cu^{2+} defects occupying the Zn^{2+} sites. In analogy, we tentatively assign the small hump A and more prominent hump B as the nn and nnn sites, respectively.

In Fig. 3(b), we summarize the temperature dependence of the intensity $I_{30\,\mu s}$ of the ^{79}Br NQR line shape integrated between 27 and 31 MHz, measured with a fixed pulse separation time $\tau = 30\ \mu$s. Also plotted in Fig. 3(b) are the integrated intensity I_o in the limit of $2\tau = 0\ \mu$s, estimated from the extrapolation of the transverse spin echo decay curves $M(2\tau)$ at the main peak presented in Figs. 2(c) and 2(d). The temperature dependence of $^{79}1/T_2$ determined from $M(2\tau)$ at $^{79}\nu_Q^{\mathrm{Main}}$ is summarized in Fig. 3(c). We confirmed that $^{79}1/T_1$ and $^{79}1/T_2$ measured at the hump A and B are comparable to the main peak's at 200 K.

The ^{79}Br NQR signals are gradually wiped out below ~150 K. The signals begin to reemerge below 75 K, followed by quick saturation at ~50 K as $^{79}1/T_2$ slows down. Notice that the main peak intensity $M(2\tau = 0)$

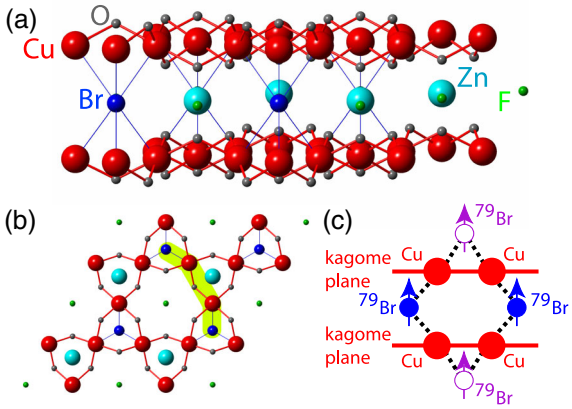

FIG. 1. (a) The structure of $ZnCu_3(OD)_6FBr$. The kagome layers consist of corner sharing triangles of Cu^{2+} ions with spin-1/2, and stacked on top of each other. For clarity, D^+ ions attached to O^{2-} are not shown. Zn^{2+}, F^-, and Br^- form the interlayer. (b) The c axis view of the kagome layer, and the interlayer underneath it. The light green shade schematically represents dimerized Br sites via a pair of Cu sites. (c) Side view of the kagome planes and ^{79}Br sites in three interlayers. Each ^{79}Br nuclear spin can couple with six nearest-neighbor ^{79}Br sites within the same interlayer (blue-blue combination) and additional six neighboring ^{79}Br sites in two adjacent kagome planes (blue-purple combination). Dashed lines represent the hyperfine coupling between ^{79}Br nuclear spin and Cu electron spin-1/2.

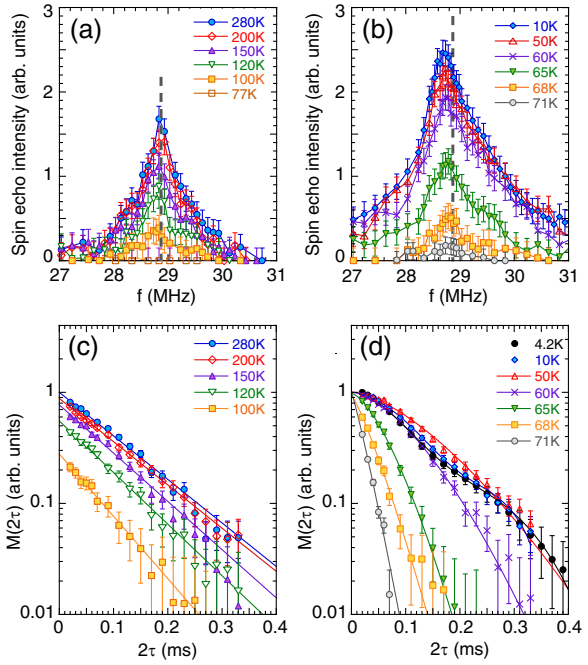

FIG. 2. Top: representative ^{79}Br NQR line shapes observed (a) above and (b) below 75 K measured with a fixed $\tau = 30\ \mu$s, corrected for the Boltzmann factor. The dashed vertical line marks the peak frequency $^{79}\nu_Q^{\mathrm{Main}} = 28.85$ MHz at 280 K. Bottom: spin echo decay curves $M(2\tau)$ observed (c) above and (d) below 75 K. The fit in (c) is with $M(2\tau) = M_o \exp\{-(2\tau/T_2)^\beta\}$ with a fixed $\beta = 1$, while $\beta(\sim 1.3)$ was allowed to vary above 50 K in (d). The solid curves through the data below 50 K represent the best two component fit with an oscillatory term, $M(2\tau) = M_o\{F\cos[\omega(2\tau)]\exp(-2\tau/D) + (1-F)\exp[-(2\tau/T_2)^\beta]\}$. The overall intensity of $M(2\tau)$ in both (c) and (d) is corrected for the Boltzmann factor, and normalized to the $M(2\tau = 0)$ value observed at 280 K.

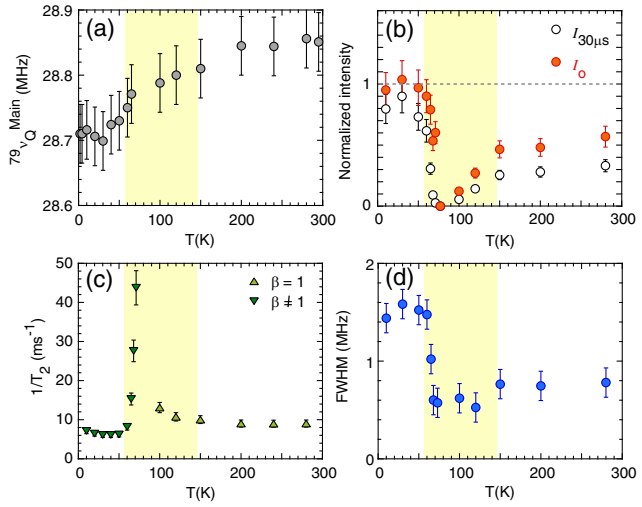

FIG. 3. (a) The main NQR peak frequency $^{79}\nu_Q^{\mathrm{Main}}$. (b) (circle) The bare integrated intensity $I_{30\ \mu s}$ of the line shapes in Figs. 2(a) and 2(b), and (orange circle) I_o at the limit of $2\tau = 0$, both corrected for the Boltzmann factor by multiplying temperature T. (c) $1/T_2$ determined from the fit in Figs. 2(c) and 2(d) with (green triangle) or without (inverted green triangle) fixing $\beta = 1$. (d) FWHM of the ^{79}Br NQR line shapes. We observe only a limited number of ^{79}Br nuclear spins due to lattice freezing in the yellow shaded region of Figs. 3 and 4.

extrapolated to $2\tau = 0$ is conserved between ~280 K and below 50 K as shown in Figs. 2(c) and 2(d), but the integrated intensity above 200 K in Fig. 3(b) is too small by a factor of ~2 compared with below 50 K.

Comparison of the ^{79}Br NQR line shapes in Figs. 2(a) and 2(b) reveals two changes across 75 K. First, the main peak frequency decreases noticeably when the signal intensity is fully recovered below 50 K, as summarized in Fig. 3(a). Second, the ^{79}Br NQR line shapes, already broad at higher temperatures, become nearly twice as broad below 50 K, as summarized in Fig. 3(d). Analogous line shape and intensity anomalies are commonly observed when spin freezing takes place in disordered magnetic materials [39]. But there is no evidence for anomalies in spin degrees of freedom around 75 K in ^{19}F NMR [15] and μSR experiments [21]. Therefore, the observed NQR anomalies must be attributed to the EFG, and we conclude that the structural environments at ^{79}Br sites become somewhat different and more disordered below ~75 K. We note that the spatially averaged crystal structure observed by diffraction techniques maintains the perfect kagome symmetry down to 3 K by neutron powder diffraction and 13 K by synchrotron x-ray diffraction [19]. Herbertsmithite also experiences a structural distortion around 50 K [7,10,12], and the interlayer Cu^{2+} defects occupying the Zn^{2+} sites may be causing it, because the ν_Q tensor at the nn ^{17}O sites changes [10]. It remains to be seen if the ~5% interlayer Cu^{2+} defects play a role in the freezing of lattice distortion in the present case. Interestingly, the ^{79}Br NQR line shapes observed below 60 K for pure barlowite $Cu_4(OH)_6FBr$ are very similar [40]. The NQR results discussed so far do not provide information on the nature of the local structural changes across 75 K, but an important clue is in the shape of the spin echo decay curve $M(2\tau)$. We will come back to this point below.

In order to understand the mechanism behind these NQR anomalies across ~75 K, we measured $^{79}1/T_1$ at the main peak between 60 and 280 K. We also measured $^{81}1/T_1$ at $^{81}\nu_Q \simeq 24.1$ MHz for the ^{81}Br sites. The $^{79,81}1/T_1$ results below 60 K were adopted from [15]. For simplicity, we deduced $1/T_1$ by fitting the nuclear spin recovery curve with the conventional stretched exponential, but more elaborate analysis based on the inverse Laplace transform (ILT) [38,41,42] leads us to the same conclusions; see Supplemental Material [38] for the details about the inverse Laplace transform T_1 analysis technique and related issues, including [41–48]. We compare $^{79}1/T_1$ and $^{81}1/T_1$ in Fig. 4(a), and summarize their ratio $R = (^{81}1/T_1)/(^{79}1/T_1)$ in Fig. 4(b). In general, $1/T_1$ measured by NQR for nuclear spin 3/2 may be expressed as $1/T_1 = 1/T_1^{\mathrm{spin}} + 1/T_1^{\mathrm{lattice}}$, where $1/T_1^{\mathrm{spin}}$ is the magnetic contribution by spin fluctuations, whereas $1/T_1^{\mathrm{lattice}}$ is caused by lattice fluctuations through the EFG. In addition, $^{79,81}1/T_1^{\mathrm{spin}}$ is proportional to the square of the nuclear gyromagnetic ratio $^{79,81}\gamma_n$, while

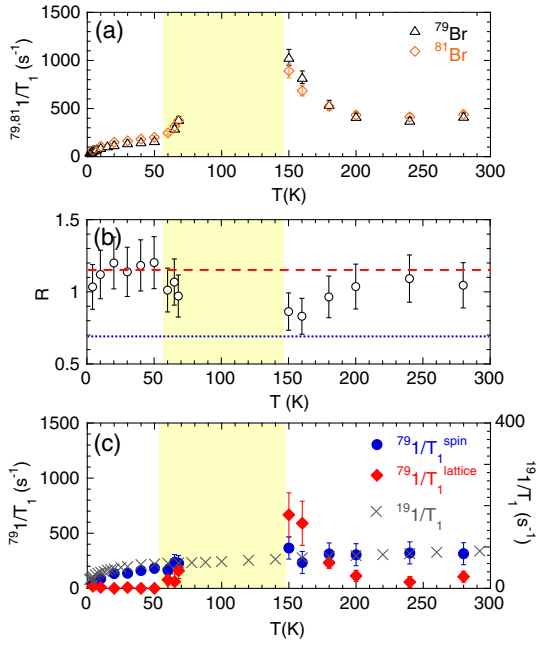

FIG. 4. (a) $^{79,81}1/T_1$ measured at the main peak. The results below 60 K were adopted from [15]. (b) The isotope ratio $R = (^{81}1/T_1)/(^{79}1/T_1)$. Dashed and dotted horizontal lines mark $R = 1.161$ (dominated by spin fluctuations) and $R = 0.698$ (dominated by lattice fluctuations). (c) $^{79}1/T_1^{\mathrm{spin}}$ and $^{79}1/T_1^{\mathrm{lattice}}$ estimated from the results in (a). Also plotted using the right axis is $^{19}1/T_1$ measured at ^{19}F sites [15].

$^{79,81}1/T_1^{\text{lattice}}$ is proportional to the square of the nuclear quadrupole moment $^{79,81}Q$, where $(^{81}\gamma_n/^{79}\gamma_n)^2 = 1.161$ and $(^{81}Q/^{79}Q)^2 = 0.698$. Therefore, the ratio $R \simeq 1.161$ observed below 50 K indicates that $^{79,81}1/T_1$ is dominated entirely by Cu spin fluctuations, but additional contributions from lattice fluctuations at the NQR frequency reduce R above 60 K.

In Fig. 4(c), we estimate $^{79}1/T_1^{\text{spin}}$ and $^{79}1/T_1^{\text{lattice}}$ separately by inserting the experimentally observed values of $^{79,81}1/T_1$ into $^{79}1/T_1 = {}^{79}1/T_1^{\text{spin}} + {}^{79}1/T_1^{\text{lattice}}$ and $^{81}1/T_1 = 1.161(^{79}1/T_1^{\text{spin}}) + 0.698(^{79}1/T_1^{\text{lattice}})$. For comparison, we also present $^{79}1/T_1^{\text{spin}}$ measured at the ^{19}F sites [15]. ^{19}F has nuclear spin 1/2 and lacks the nuclear quadrupole moment, hence probes only spin fluctuations with no influence of the EFG. The similarity in the observed temperature dependence between $^{79}1/T_1^{\text{spin}}$ and $^{19}1/T_1$ assures us that our procedures to separate $^{79}1/T_1$ into $^{79}1/T_1^{\text{spin}}$ and $^{79}1/T_1^{\text{lattice}}$ are working well.

One of the key findings of the present Letter is that $^{79}1/T_1^{\text{lattice}}$ undergoes a drastic enhancement below the temperature scale set by $J \simeq 160$ K. Intuitively, this is easily understandable. When the temperature is lowered below J, neighboring Cu sites become magnetically frustrated, because three Cu spin-1/2's located at the corners of each triangle cannot form singlets all at once. The effects of this magnetic frustration can be partially alleviated if the lattice distorts and two sites form a dimer at the cost of enhanced elastic energy. Combined with the aforementioned changes observed for $^{79}\nu_Q$ and its distributions, the $^{79}1/T_1^{\text{lattice}}$ results, therefore, suggest that magnetic frustration effects play a role in enhancing structural distortions below temperature $\sim J$ through the magnetoelastic coupling effects [49]. The NQR signal is completely wiped out around 75 K, when the spectral weight of the EFG fluctuations becomes very large around the NQR frequency and enhances $^{79}1/T_1$ and $^{79}1/T_2$; the NQR signals reemerge below 75 K, because the EFG fluctuations become slower than the NQR frequency. Once the EFG becomes completely static below 50 K at the NQR measurement time scale of ~ 0.04 μs, the NQR intensity saturates and $^{79}1/T_1^{\text{lattice}}$ vanishes. We also emphasize that 100% of the sample volume is affected by these EFG anomalies, which is why the entire ^{79}Br NQR signal intensity is wiped out.

The T_2 results summarized in Figs. 2(c), 2(d), and 3(c) provide additional support for the physical picture described in the previous paragraph. Notice that the spin echo decay curve $M(2\tau)$ below 50 K exhibits a typical Gaussian-Lorentzian form with a negative curvature below $2\tau \sim 0.1$ ms. This is typical for solids, and consistent with the frozen state of the lattice. But $^{79}1/T_2$ is strongly enhanced above 60 K, and the $M(2\tau)$ curves become almost Lorentzian (i.e., exponential). This is consistent with the motional narrowing effects [29,33] induced by the slowly fluctuating EFG. The spin echo decay is also nearly Lorentzian above 100 K up to 280 K, hinting the possibly dynamic nature of the lattice even above $T \sim J$. It might also explain why the integrated intensity above 200 K is too small by a factor of ~ 2.

A striking aspect of Fig. 2(d) is that $M(2\tau)$ develops a damped oscillatory component $F\cos[\omega_o(2\tau)]\exp(-2\tau/D)$ in the frozen state below 50 K, preceding the gradual emergence of Cu-Cu spin singlets below ~ 30 K [15]. Here, $\omega_o \simeq 20$ ms^{-1} and $D \simeq 0.1$ ms represent the oscillation frequency and damping time constant, respectively, and the fraction of the oscillatory component reaches $F \sim 0.25$ at 4.2 K.

Analogous oscillatory behaviors were previously reported for spin singlets in dimerized materials $SrCu_2(BO_3)_2$ [30] and $Cu_2Sc_2Mg_4O_{13}$ [31] with the oscillation frequency $\omega_o = A_{hf}^2/4J$ set by the intradimer super exchange J [34] (A_{hf} represents the hyperfine coupling between the observed nuclear spin and Cu electron spin, which is unknown for Zn-barlowite). In these dimerized materials, the hyperfine magnetic field generated by a ^{63}Cu nuclear spin $\hat{\mathbf{I}}_i$ induces singlet-triplet excitation in a pair of Cu electron spins, which, in turn, induces a hyperfine magnetic field on another ^{63}Cu nuclear spin $\hat{\mathbf{I}}_j$, resulting in a Ruderman-Kittel-Kasuya-Yosida-like indirect nuclear spin-spin coupling [32] between two ^{63}Cu nuclear spins. In analogy, the oscillatory behavior of $M(2\tau)$ below 50 K indicates that some of the Br sites form a dimerized cluster linked by a Cu-Cu bond, as schematically depicted with light green shade in Fig. 1(b). We conducted preliminary spin echo decay measurements at ^{63}Cu sites [50], and confirmed that ^{63}Cu also exhibits a damped oscillation with frequency ω_o similar to $Cu_2Sc_2Mg_4O_{13}$ (with comparable $J \simeq 260$ K [51]). Therefore, we conclude that the spin echo amplitude oscillations observed below ~ 50 K reflect the formation of Br-Cu-Cu-Br clusters, which may be related to our prior observation of the gradual emergence of Cu spin singlets below ~ 30 K [15].

In general, the oscillation of spin echo amplitude can occur only if we use radio frequency pulses to flip a pair of so-called like spins resonating at the same frequency [34,35]; this means that we need to flip a pair of ^{79}Br-^{79}Br nuclear spins, rather than a pair of unlike spins, ^{79}Br-^{81}Br. Since the natural abundance of ^{79}Br is 51%, the maximum possible oscillation amplitude is, therefore, $0.51M(2\tau = 0)$ for ^{79}Br NQR. Accordingly, $F \sim 0.25$ at 4.2 K implies that the actual fraction of the ^{79}Br sites involved in the clusters may be as large as $F/0.51 \sim 0.5$.

It is important to recall, however, that the oscillation of $M(2\tau)$ at low temperatures persists many cycles with little damping in the case of well-isolated spin dimers in $SrCu_2(BO_3)_2$ [30] and $Cu_2Sc_2Mg_4O_{13}$ [31]. On the other hand, $M(2\tau)$ observed for two-leg spin ladders in

$SrCu_2O_3$ [36] and $Sr_{14}Cu_{24}O_{41}$ [37] exhibits a Gaussian form of decay without oscillations, despite the singlet formation along the rung. This is because many spin singlets are entangled along the legs, resulting in superposition of many different oscillation frequencies a_{ij}, and their average becomes a Gaussian [34,35]. In other words, if the spin singlets that emerge below ~30 K in Zn-barlowite [15] are isolated in the present case [as in $SrCu_2(BO_3)_2$ and $Cu_2Sc_2Mg_4O_{13}$], we expect a well defined oscillation with little damping, whereas entanglement of many singlets would lead to a Gaussian (as in $SrCu_2O_3$ and $Sr_{14}Cu_{24}O_{41}$). The oscillation observed for Zn-barlowite has a clearly defined frequency but with strong damping and is somewhere between these two extreme cases. This underscores the disordered nature of the magnetic ground state in this material. Note that, theoretically, both nearly isolated and entangled singlets may coexist within a disordered kagome plane [26]. A potential caveat of these arguments is that each ^{79}Br can, in principle, form a large cluster and couple with up to six ^{79}Br sites within the same interlayer and an additional six ^{79}Br sites in the two adjacent interlayers above and below, as shown in Fig. 1(c). Simultaneous indirect couplings with many ^{79}Br sites would cause strong damping in the oscillation. But diffraction experiments have not detected evidence for such large cluster formation.

To summarize, we used ^{79}Br NQR to demonstrate that the lattice degrees of freedom in Zn-barlowite undergo gradual freezing below $J \sim 160$ K. In the frozen state below 50 K, the lattice becomes static with additional structural disorder at local levels. The oscillation of the spin echo decay induced by indirect nuclear spin-spin interaction indicates that up to ~50% of Br sites in the frozen state are involved in structural dimer formation encompassing Cu-Cu pairs. The strong damping of oscillation is inconsistent with completely isolated Cu spin dimers formed in the kagome planes. On the other hand, a well-defined period of oscillation suggests that Cu spin singlets are not as strongly entangled as in two-leg spin ladders, which exhibit Gaussian decay, instead. The mixed response that we observed is consistent with the notion of closely competitive states in Zn-barlowite that are strongly perturbed by local disorder.

T. I. thanks K. Yoshimura for helpful communications, and Y. Itoh for critical reading of the manuscript. The work at McMaster was supported by NSERC (T. I.). P. M. S. was supported by the Rice University Consortium for Processes in Porous Media. The work at Stanford and SLAC (sample synthesis and characterization) was supported by the U.S. Department of Energy (DOE), Office of Science, Basic Energy Sciences, Materials Sciences and Engineering Division, under Contract No. DE-AC02-76SF00515 (Y. S. L. and J. W.). R. W. S. was supported by a NSF Graduate Research Fellowship (Grant No. DGE-1656518).

[1] L. Balents, Nature (London) **464**, 199 (2010).
[2] C. Broholm, R. J. Cava, S. A. Kivelson, D. G. Nocera, M. R. Norman, and T. Senthil, Science **367**, 263 (2020).
[3] M. P. Shores, E. A. Nytko, B. M. Bartlett, and D. G. Nocera, J. Am. Chem. Soc. **127**, 13462 (2005).
[4] J. S. Helton, K. Matan, M. P. Shores, E. A. Nytko, B. M. Bartlett, Y. Yoshida, Y. Takano, A. Suslov, Y. Qiu, J.-H. Chung, D. G. Nocera, and Y. S. Lee, Phys. Rev. Lett. **98**, 107204 (2007).
[5] D. E. Freedman, T.-H. Han, A. Prodi, P. Muller, Q.-Z. Huang, Y.-H. Chen, S. M. Webb, Y. S. Lee, T. M. mcQueen, and D. G. Noera, J. Am. Chem. Soc. **132**, 16185 (2010).
[6] T.-H. Han, J. S. Helton, S. Chu, D. G. Nocera, J. A. Rodriguez-Rivera, C. Broholm, and Y. S. Lee, Nature (London) **492**, 406 (2012).
[7] T. Imai, E. A. Nytko, B. M. Bartlett, M. P. Shores, and D. G. Nocera, Phys. Rev. Lett. **100**, 077203 (2008).
[8] A. Olariu, P. Mendels, F. Bert, F. Duc, J. C. Trombe, M. A. de Vries, and A. Harrison, Phys. Rev. Lett. **100**, 087202 (2008).
[9] T. Imai, M. Fu, T. H. Han, and Y. S. Lee, Phys. Rev. B **84**, 020411(R) (2011).
[10] M. Fu, T. Imai, T.-H. Han, and Y. S. Lee, Science **350**, 655 (2015).
[11] T.-H. Han, M. R. Norman, J.-J. Wen, J. A. Rodriguez-Rivera, J. S. Helton, C. Broholm, and Y. S. Lee, Phys. Rev. B **94**, 060409(R) (2016).
[12] A. Zorko, M. Herak, M. Gomilšek, J. van Tol, M. Velázquez, P. Khuntia, F. Bert, and P. Mendels, Phys. Rev. Lett. **118**, 017202 (2017).
[13] I. Kimchi, J. P. Sheckelton, T. M. McQueen, and P. Lee, Nat. Commun. **9**, 4367 (2018).
[14] P. Khuntia, M. Velazquez, Q. Barthélemy, F. Bert, E. Kermarrec, A. Legros, B. Bernu, L. Messio, A. Zorko, and P. Mendels, Nat. Phys. **16**, 469 (2020).
[15] J. Wang, W. Yuan, P. M. Singer, R. W. Smaha, W. He, J. Wen, Y. S. Lee, and T. Imai, Nat. Phys. **17**, 1109 (2021).
[16] Y. Y. Huang, Y. Xu, L. Wang, C. C. Zhao, C. P. Tu, J. M. Ni, L. S. Wang, B. L. Pan, Y. Fu, Z. Hao, C. Liu, J.-W. Mei, and S. Y. Li, Phys. Rev. Lett. **127**, 267202 (2021).
[17] H. Murayama, T. Tominaga, A. Asaba, T. de Oliveira Silva, Y. Sato, H. Suzuki, Y. Ukai, S. Suetsugu, Y. Kasahara, R. Okuma, I. Kimchi, and Y. Matsuda, arXiv:2106.07223.
[18] Z. Feng, Z. Li, X. Meng, W. Yi, Y. Wei, J. Zhang, Y.-C. Wang, W. Jiang, Z. Liu, S. Li, F. Liu, J. Luo, S. Li, G. qing Zheng, Z. Y. Meng, J.-W. Mei, and Y. Shi, Chin. Phys. Lett. **34**, 077502 (2017).
[19] R. W. Smaha, W. He, J. M. Jiang, J. Wen, Y.-F. Jiang, J. P. Sheckelton, C. Titus, S. G. Wang, Y. Chen, S. J. Teat, A. A. Aczel, Y. Zhao, G. Xu, J. W. Lynn, H.-C. Jiang, and Y. S. Lee, npj Quantum Mater. **5**, 23 (2020).
[20] R. W. Smaha, I. Boukahil, C. J. Titus, J. M. Jiang, J. P. Sheckelton, W. He, J. Wen, J. Vinson, S. G. Wang, Y.-S. Chen, S. J. Teat, T. P. Devereaux, C. D. Pemmaraju, and Y. S. Lee, Phys. Rev. Mater. **4**, 124406 (2020).
[21] K. Tustain, B. Ward-O'Brien, F. Bert, T.-H. Han, H. Luetkens, T. Lancaster, B. M. Huddart, P. J. Baker, and L. Clark, npj Quantum Mater. **5**, 74 (2020).
[22] Y. Fu, M.-L. Lin, L. Wang, Q. Liu, L. Huang, W. Jiang, Z. Hao, C. Liu, H. Zhang, X. Shi, J. Zhang, J. Dai, D. Yu,

F. Ye, P. A. Lee, P.-H. Tan, and J.-W. Mei, Nat. Commun. **12**, 3048 (2021).
[23] K. Tustain, E. E. McCabe, A. M. Arevalo-Lopez, A. S. Gibbs, S. P. Thompson, C. A. Murray, C. Ritter, and L. Clark, Chem. Mater. **33**, 9638 (2021).
[24] H. Kawamura, K. Watanabe, and T. Shimokawa, J. Phys. Soc. Jpn. **83**, 103704 (2014).
[25] T. Shimokawa, K. Watanabe, and H. Kawamura, Phys. Rev. B **92**, 134407 (2015).
[26] H. Kawamura and K. Uematsu, J. Phys. Condens. Matter **31**, 504003 (2019).
[27] R. R. P. Singh, Phys. Rev. Lett. **104**, 177203 (2010).
[28] E. L. Hahn and D. E. Maxwell, Phys. Rev. **88**, 1070 (1952).
[29] A. Abragam, *The Principles of Nuclear Magnetism* (Oxford University Press, Oxford, 1961).
[30] K. Kodama, J. Yamazaki, M. Takigawa, H. Kageyama, K. Onizuka, and Y. Ueda, J. Phys. Condens. Matter **14**, L319 (2002).
[31] J. Kikuchi, S. Nagura, H. Nakanishi, and T. Masuda, J. Phys. Conf. Ser. **200**, 022024 (2010).
[32] M. A. Ruderman and C. Kittel, Phys. Rev. **96**, 99 (1954).
[33] C. P. Slichter, *Principles of Magnetic Resonance*, 3rd ed. (Springer, New York, 2010).
[34] C. H. Pennington, D. J. Durand, C. P. Slichter, J. P. Rice, E. D. Bukowski, and D. M. Ginsberg, Phys. Rev. B **39**, 274 (1989).
[35] C. H. Pennington and C. P. Slichter, Phys. Rev. Lett. **66**, 381 (1991).
[36] K. Ishida, Y. Kitaoka, Y. Tokunaga, S. Matsumoto, K. Asayama, M. Azuma, Z. Hiroi, and M. Takano, Phys. Rev. B **53**, 2827 (1996).
[37] M. Takigawa, N. Motoyama, H. Eisaki, and S. Uchida, Phys. Rev. B **57**, 1124 (1998).
[38] See Supplemental Material at http://link.aps.org/supplemental/10.1103/PhysRevLett.128.157202 for additional details about the sample, data, and analysis.
[39] A. W. Hunt, P. M. Singer, A. F. Cederström, and T. Imai, Phys. Rev. B **64**, 134525 (2001).
[40] K. M. Ranjith, C. Klein, A. A. Tsirlin, H. Rosner, C. Krellner, and M. Baenitz, Sci. Rep. **8**, 10851 (2018).
[41] J. Mitchell, T. C. Chandrasekera, and L. Gladden, Prog. Nucl. Magn. Reson. Spectrosc. **62**, 34 (2012).
[42] P. M. Singer, A. Arsenault, T. Imai, and M. Fujita, Phys. Rev. B **101**, 174508 (2020).
[43] A. Arsenault, T. Imai, P. M. Singer, K. M. Suzuki, and M. Fujita, Phys. Rev. B **101**, 184505 (2020).
[44] S. K. Takahashi, J. Wang, A. Arsenault, T. Imai, M. Abramchuk, F. Tafti, and P. M. Singer, Phys. Rev. X **9**, 031047 (2019).
[45] J. Wang, W. Yuan, T. Imai, P. M. Singer, F. Bahrami, and F. Tafti, Phys. Rev. B **103**, 214405 (2021).
[46] D. C. Johnston, S.-H. Baek, X. Zong, F. Borsa, J. Schmalian, and S. Kondo, Phys. Rev. Lett. **95**, 176408 (2005).
[47] E. R. Andrew and D. P. Tunstall, Proc. Phys. Soc. London **78**, 1 (1961).
[48] A. Narath, Phys. Rev. **162**, 320 (1967).
[49] Y. Li, A. Pustogow, M. Bories, P. Puphal, C. Krellner, M. Dressel, and R. Valentí, Phys. Rev. B **101**, 161115(R) (2020).
[50] J. Wang *et al.* (to be published).
[51] J. Kikuchi, S. Nagura, K. Murakami, T. Masuda, and G. J. Redhammer, J. Phys. Soc. Jpn. **82**, 034710 (2013).